Signatures of chaos in strong-field double ionization

Francois Mauger, Cristel Chandre, Turgay Uzer

Signatures of chaos in strong-field double ionization

F. Mauger[1], C. Chandre[1], T. Uzer[2]
[1] *Centre de Physique Théorique, CNRS – Aix-Marseille Université, Campus de Luminy, case 907, F-13288 Marseille cedex 09, France*
[2] *School of Physics, Georgia Institute of Technology, Atlanta, GA 30332-0430, USA*

When intense laser pulses release correlated electrons, the time delay between the ionizations may last more than half a laser period. We show that this "Recollision-Excitation with Subsequent Ionization" pathway originates from chaotic dynamics in the double ionization process. The long delays after the first ionization are caused by "sticky" regions in phase space, and the unstable manifold of a particular periodic orbit regulates the second ionization. The oscillations observed in the corresponding double ionization yields versus the laser intensity are a signature of chaotic processes in two-active electron systems.

PACS numbers: 32.80.Rm, 05.45.Ac

Atoms in strong laser pulses lose their electrons through two ionization channels [1]: A sequential one (SDI) and its non-sequential counterpart (NSDI). The SDI mechanism consists of successive and independent removals of the two electrons. The recollision (or three-step) scenario [2, 3] in which an ionized electron returns to the ion core to dislodge a bound electron is the characteristic mechanism for NSDI. In contrast to SDI, the latter mechanism is driven by electron correlation. It turns out that there is a rich variety of pathways among NSDI processes, also. At first sight, these pathways can be distinguished by the time it takes the second electron to ionize. The common variant involves little, if any, delay between the recollision and ionization. However, this so-called "direct impact ionization" [4] is often accompanied by an alternative (and less straightforward) road to NSDI called Recollision-induced Excitation with Subsequent Ionization (or RESI for short [4–7]): The recollision excites the parent ion which is ionized by the laser field after some delay, sometimes lasting longer than half a laser cycle after the recollision and therefore imitating an uncorrelated ionization process. RESI processes have been computed quantum mechanically [8–10] and classically [11–13]. Fortunately one does not need to rely on vague criteria like length of delay when distinguishing these pathways since they carry distinct signatures in their ion momentum distributions: The two lateral peaks in the bimodal distribution come from direct ionization whereas the central part around zero ion momentum is due to RESI [4, 5, 8, 14, 15]. It also turns out that direct impact ionization takes place when the electric field is close to zero whereas RESI when the electric field is maximum.

In this Letter, we investigate the phase-space mechanisms of RESI. We show that RESI is organized by a small number of periodic orbits and their manifolds [16] that, in a manner of speaking, "funnel" the ionizing electrons away from the ion core in specific ways. These structures are embedded in a "sticky" (chaotic) region [17] that traps some trajectories before ionizing. While we present numerical results for neon, we find that the same qualitative mechanism holds for other two active electron systems as well. In particular, our dynamical treatment confirms that the second ionization in RESI happens at the maxima of the field irrespective of the atom considered.

Remarkably, classical mechanics can identify both pathways that lead to double ionization (as well as RESI) and reproduce the experimental and computational observations closely [18–20]. Classical models scale advantageously with system size, and detailed trajectories can reveal the underlying mechanisms. Here we complement the three-step picture [2, 3] with an analysis of the core electron dynamics. Indeed, it turns out that the dynamics of the remaining ion after a recollision is pivotal in understanding the mechanisms at play in the subsequent ionization processes [20].

We consider a two active electron atom with soft-Coulomb potentials subjected to an intense and short linearly polarized laser pulse in the dipole approximation [18–20]. The relevant dynamics of this standard model takes place along the polarization axis that permits a Hamiltonian model with a single spatial dimension [18, 21–23]:

$$\begin{aligned}\mathcal{H}(x_1,x_2,p_1,p_2,t) = \frac{p_1^2}{2}+\frac{p_2^2}{2}-\frac{2}{\sqrt{x_1^2+a^2}}\\ -\frac{2}{\sqrt{x_2^2+a^2}}+\frac{1}{\sqrt{(x_1-x_2)^2+b^2}}\\ +(x_1+x_2)\,E_0 f(t)\sin\omega t,\end{aligned} \tag{1}$$

where x_i is the position of the ith electron (the nucleus is assumed to be fixed at the origin) and p_i is its canonically conjugate momentum. The laser field is characterized by its amplitude E_0 and has a wavelength of 780 nm ($\omega = 0.0584$ a.u.) with a trapezoidal shape f consisting of two-cycle linear ramp up and six laser cycle constant plateau. The constants a and b are the electron-nucleus and electron-electron softening parameters [18, 21–23] respectively and are chosen so as to be compatible with the ground state energy $\mathcal{E}_g$.

RESI events are described by two-electron trajectories for which, after a recollision, one electron remains bound

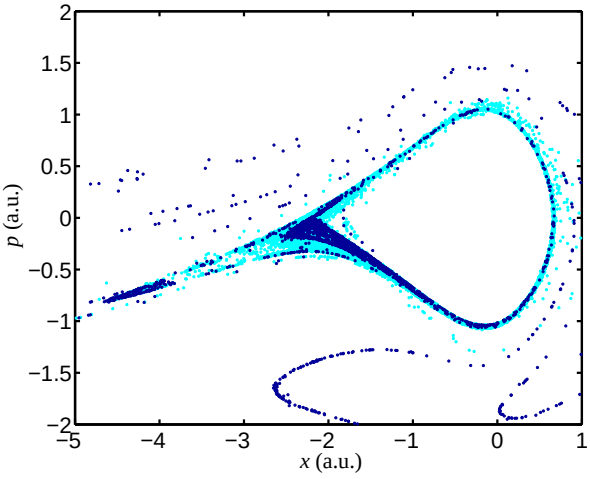

FIG. 1: Poincaré section (stroboscopic plot at the maximum of the field, $\phi = \pi/2$) of RESI trajectories, after the last recollision, obtained for the two active electron model (1) of neon [18–20] for $I = 3 \times 10^{15}\mathrm{W \cdot cm^{-2}}$ during the plateau of the laser. The parameters are $a = 1$ and $b = 1$ and the initial conditions have a microcanonical distribution on the energy surface $\mathcal{E}_g = -2.3$ a.u. For each RESI, the first point on the section is plotted in light blue while the following ones are in dark blue.

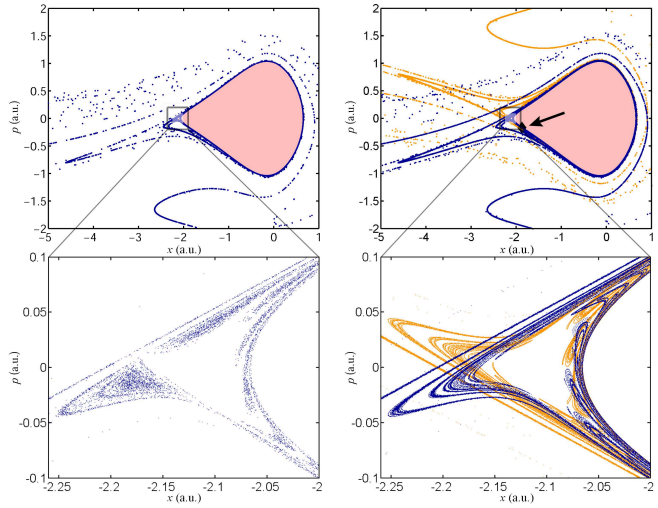

FIG. 2: Left panels: Poincaré section (stroboscopic plots at the maximum of the laser field, i.e. $\phi = \pi/2$) of RESI trajectories of the one-electron reduced Hamiltonian (2) for Ne^+ detected from a large set of random initial conditions for a laser intensity $I = 3 \times 10^{15}$ W $\cdot$ cm^{-2}. Right panels: Poincaré section (with the same surface of section and laser intensity as the left panels) of the stable (light orange dots) and unstable (dark blue dots) manifolds of the periodic orbit $\mathcal{O}_a$ of Hamiltonian (2). The position of the periodic orbit $\mathcal{O}_a$ is indicated with a black diamond (see the arrow) in the upper right panel. The pink area in the upper panels represents the part of phase space from which the inner electron does not ionize. The lower panels focus on specific parts of the phase space depicted in the upper panels.

to the nucleus for a long time before ionizing without any additional recollision, i.e., without the other electron ever returning to the nucleus. We use an energy criterion to designate an electron as ionized or not [20, 22, 24]. A recollision is said to have occurred whenever the distance between the two electrons is smaller (or equivalently, whenever the Coulomb interaction between the two electrons is larger) than some threshold. We consider the NSDI trajectories which double-ionize after a (last) recollision. In some of these, the RESIs, one electron leaves the nucleus long after the first electron has left that region. For the computation, we choose a time delay of at least half of a laser cycle between the last recollision and the ionization of the remaining ion. Poincaré sections of RESI trajectories are depicted in Fig. 1 for Hamiltonian (1). Looking at the swirling patterns that compose these trajectories, it is natural to ask: Why do trajectoies follow these complicated paths?

This question is best answered using a single atomic electron model (Ne^+ for instance): A recollision has excited the inner electron while the recolliding electron remains ionized [20] [which allows us to neglect the electron-electron interaction in Hamiltonian (1)]. The resulting reduced-dimensional Hamiltonian with one and a half degrees of freedom reads

$$\mathcal{H}(x,p,t) = \frac{p^2}{2} - \frac{2}{\sqrt{x^2+a^2}} + xE_0 \sin(\omega t + \phi_0), \quad (2)$$

where ϕ_0 denotes the phase at which the last recollision occurs [25]. RESI are obtained by imposing the following requirements to trajectories of Hamiltonian (2), initiated randomly: They are those for which the electron ionizes at the end of the laser pulse and, during (at least) half of a laser cycle it remains bound to the nucleus. In the left panels of Fig. 2, we represent Poincaré sections (stroboscopic plots at the maximum of the laser, i.e., $\phi \equiv \omega t + \phi_0 \mod 2\pi = \pi/2$) of all the RESI trajectories that were detected according to the above criteria for Hamiltonian (2). For clarity we left out the two first points on the Poincaré section for each detected RESI (the missing points are located in the same part of phase space as the remaining ones, but they clutter the fine structures depicted on the figure). Note the close similarity between the Poincaré section of trajectories of the two-electron system (1) in Fig. 1 and the ones of the reduced one electron system (2) in Fig. 2 (upper left panel). In particular the filamented patterns in both figures stand out.

The dynamics given by Hamiltonian (2) in phase space is the key to the patterns formed by the RESI trajectories. Previous studies on Hamiltonian (2) [20, 24] have yielded two qualitatively different kinds of dynamics for the electron driven by the field: In the competition between Coulomb attraction to the nucleus and the laser excitation, either the latter prevails, and the electron is quickly ionized; or the Coulomb attraction manages to

maintain the electron trapped near the core [27]. Two areas in phase space emerge from this distinction: A bound area, close to the nucleus (pink area in Fig. 2, upper panels), where the electron is trapped by the nucleus and cannot ionize; and an unbound area, further away (white area in the same panels), where the electron is quickly ionized by the laser. Loosely speaking, one can almost certainly predict the electron's fate from its starting position in phase space: Un-ionized if it starts in the bound area (colored pink in Fig. 2, upper panels) or ionized if it starts in the unbound area (outside the pink region). The comparatively long ionization times stem from the RESI trajectories starting from the edge of the bound area. A more detailed study shows that the behavior in the unbound region is more complex than anticipated. This is readily observed by the patterns present in the unbound region in Fig. 2. The rich dynamics in that region is caused by the structures observed for the RESI trajectories, as we shall see below.

A thin chaotic transition layer of phase space in the unbound region, and located outside the last invariant torus that defines the bound region, is responsible for RESI. This region is filled with periodic orbits, invariant tori (in small elliptic islands), cantori, stable and unstable manifolds of hyperbolic orbits, etc... In what follows, we show that this transition region, at a given intensity, is organized by a small number (between one and three) of hyperbolic periodic orbits. All those periodic orbits are created by the main resonances of the free field dynamics [$E_0 = 0$ in Hamiltonian (2)] and the laser (the resonant periodic orbits have the same period as the laser). Since they are linked by symmetry we need to consider only one of them. We denote that periodic orbit by $\mathcal{O}_a$.

The behavior around $\mathcal{O}_a$ depends strongly on its location, linear, and nonlinear stability properties. To analyze the nonlinear properties of this orbit, and to understand how $\mathcal{O}_a$ organizes effectively the dynamics in the transition region, we compute the stable and unstable manifolds of the hyperbolic periodic orbit $\mathcal{O}_a$ and display the resulting pictures in Fig. 2 (right panels). These are the pathways by which the electrons approach or leave the core. Note the strong similarities of the unstable manifold of $\mathcal{O}_a$ with the Poincaré sections of RESI trajectories in Fig. 1. This similarity confirms the important role played by this unstable manifold in the RESI process. Looking at Fig. 2, we see that the stable and unstable manifolds associated with $\mathcal{O}_a$ develop around the bound area. Parts of these manifolds are in the close vicinity of the bound region, and branches extend deep into the unbound region. Besides, the thinness of those manifolds explains why the transition between the bound and unbound areas is so sharp [20]. In addition, we see that the stable and unstable manifolds intersect an infinite number of times, a characteristic feature of a chaotic dynamics [28]. A comparison between the left and right panels of Fig. 2 (obtained for an intensity $I = 3 \times 10^{15}$ W $\cdot$ cm^{-2}) shows that the unstable manifold of $\mathcal{O}_a$ regulates the dynamics of the RESI trajectories; even some of the very fine details of the unstable manifold are reproduced by this set of RESI trajectories. We note that parts of the unstable manifold are missing: They correspond to the intersections between the stable and the unstable manifolds. The overlap between the stable and unstable manifolds of $\mathcal{O}_a$ forms a "sticky" region [17] that traps trajectories for some time before ionizing. There are other periodic orbits in the vicinity of the bound area, but they influence only the fine details of the chaotic structure.

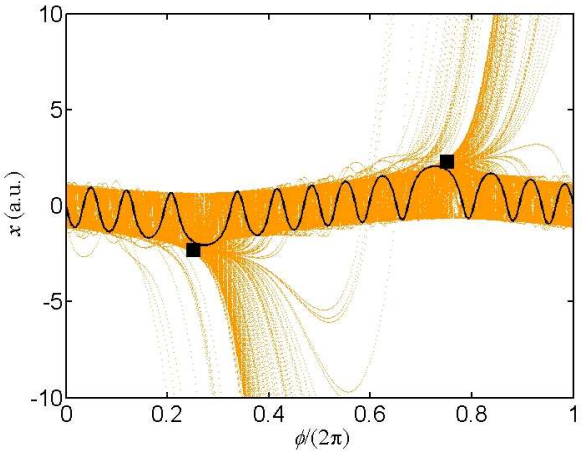

FIG. 3: Projection of the unstable manifold of the periodic orbit $\mathcal{O}_a$ of Hamiltonian (2) for $I = 3 \times 10^{15}$ W $\cdot$ cm^{-2} in the (x, ϕ) plane. The black curve is a projection of the periodic orbit $\mathcal{O}_a$ in the plane (x, ϕ), and the black squares indicate the position of the saddle point at the maximum of the field.

For deeper insight into the shape of the unstable manifold of $\mathcal{O}_a$, we represent a projection of this manifold in the plane (x, ϕ) together with a projection of $\mathcal{O}_a$ (black curve) in Fig. 3. It shows a central region near $x = 0$ and two main branches which depart from this central region. It is worth noticing that these branches are located near the extrema of the electric field, i.e., when $\phi = \pi/2$ and $\phi = 3\pi/2$. Since a RESI trajectory follows asymptotically this unstable manifold, we see that this trajectory will leave the nucleus at times that correspond to the extrema of the electric field. This is consistent with what is already observed [8]. The unstable manifold has some other branches through which an electron can leave the nucleus and that do not correspond to extrema of the electric field. However, the probability of those ionization channels is much smaller.

The bound region shrinks with increasing laser intensity, and higher-order resonant periodic orbits are drawn to the unbound region. To investigate the impact of these orbits on RESI, we compute the proportion of RESI relative to the double ionization yield of Hamiltonian (1) when the intensity of the laser is varied. These yields are compared with the stability index [16] of the resonant periodic orbits identified from the reduced model (2). The

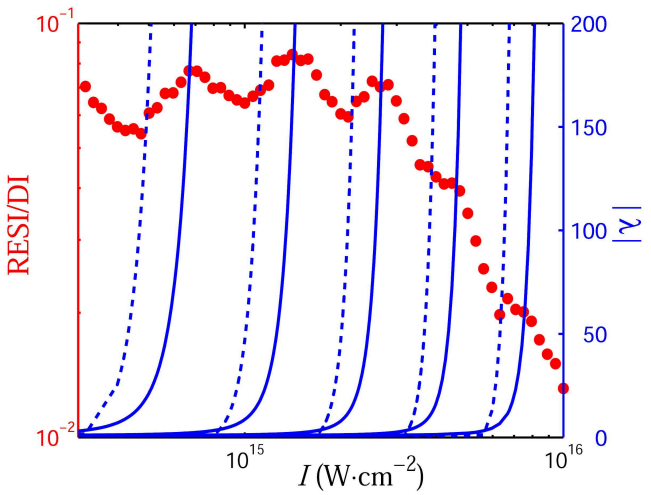

FIG. 4: Proportion of RESI relative to the double ionization yield for neon (red dots, left hand y-axis) obtained from Hamiltonian (1) and linear stability index [16] of the resonant periodic orbits of Hamiltonian (2) (blue curves, right hand y-axis) as functions of the laser intensity I. Continuous and broken curves refer to odd and even $(1:n)$ resonances, respectively (see text).

stability index measures the typical time this orbit is expected to influence the neighboring dynamics: The larger the stability index, the sooner a neighboring trajectory will diverge from it. The resulting picture is displayed in Fig. 4 for neon. It shows that, in the nonsequential double ionization regime the proportion of RESI oscillates around an almost constant value. These oscillations are a clear signature of the resonant periodic orbits of the reduced Hamiltonian (2) which organize the chaotic layer around the bound region.

The same analysis can be carried out for other two-active-electron atoms by varying the ground state energy and adjusting the softening parameters. In particular, for helium, neon, and argon we have found that the RESI process is organized by the same resonant periodic orbits. Our findings suggest that the differences in the momentum spectra as observed for various atoms in Ref. [4, 6, 7] do not come from the phase space structures that regulate RESI. Since the relative amount of RESI versus NSDI is fairly similar for all three atoms and does not depend strongly on the intensity in the NSDI regime, the origin of these differences must be sought in the proportion of SDI versus NSDI in various intensity regimes.

In summary, we have shown that the process of RESI is a signature of a chaotic behavior resulting from the competition between the laser field and the attraction to the nucleus. This mechanism holds irrespectively of the atom, and it persists all over the nonsequential double ionization regime. The oscillations observed in Fig. 4 are one of the few signatures of chaos in the dynamics of two active electron atoms subjected to strong laser pulses.

C.C. and F.M. acknowledge financial support from the PICS program of the CNRS. This work is partially funded by NSF.

[1] W. Becker and H. Rottke, Contemporary Physics **49**, 199 (2008).
[2] P. B. Corkum, Phys. Rev. Lett. **71**, 1994 (1993).
[3] K. J. Schafer *et al.*, Phys. Rev. Lett. **70**, 1599 (1993).
[4] A. Rudenko *et al.*, Phys. Rev. Lett. **93**, 253001 (2004).
[5] B. Feuerstein *et al.*, Phys. Rev. Lett. **87**, 043003 (2001).
[6] V. L. B. de Jesus *et al.*, J. Elec. Spect. **141**, 127 (2004).
[7] V. L. B. de Jesus *et al.*, J. Phys. B. **37**, L161 (2004).
[8] C. Ruiz and A. Becker, New J. Phys. **10**, 025020 (2008).
[9] S. Baier, A. Becker, and L. Plaja, Phys. Rev. A **78**, 013409 (2008).
[10] T. Shaaran, M. T. Nygren, and C. Figueira de Morisson Faria, Phys. Rev. A **81**, 063413 (2010).
[11] S. L. Haan, J. S. Van Dyke, and Z. S. Smith, Phys. Rev. Lett. **101**, 113001 (2008).
[12] K. N. Shomsky, Z. S. Smith, and S. L. Haan, Phys. Rev. A **79**, 061402(R) (2009).
[13] S. L. Haan *et al.*, Phys. Rev. A **81**, 023409 (2010).
[14] T. Weber, *et al.*, Phys. Rev. Lett. **84**, 443 (2000).
[15] R. Moshammer *et al.*, Phys. Rev. Lett. **84**, 447 (2000).
[16] P. Cvitanović, R. Artuso, R. Mainieri, G. Tanner, and G. Vattay, *Chaos: Classical and Quantum* (Niels Bohr Institute, Copenhagen, 2008), `http://ChaosBook.org`.
[17] G. Contopoulos, *Order and Chaos in Dynamical Astronomy* (Springer, Berlin 2002), ISBN 978-3-540-43360-6.
[18] R. Panfili and J. H. Eberly, Opt. Express **8**, 431 (2001).
[19] P. J. Ho *et al.*, Phys. Rev. Lett. **94**, 093002 (2005).
[20] F. Mauger, C. Chandre, and T. Uzer, Phys. Rev. Lett. **102**, 173002 (2009); J. Phys. B. **42**, 165602 (2009).
[21] J. Javanainen, J. H. Eberly, and Q. Su, Phys. Rev. A **38**, 3430 (1988).
[22] R. Panfili, S. L. Haan, and J. H. Eberly, Phys. Rev. Lett. **89**, 113001 (2002).
[23] S. L. Haan, R. Grobe, and J. H. Eberly, Phys. Rev. A **50**, 378 (1994).
[24] F. Mauger, C. Chandre, and T. Uzer, Phys. Rev. Lett. **104**, 043005 (2010); Phys. Rev. A **81**, 063425 (2010).
[25] This one-electron version of the two-electron Hamiltonian bears a superficial similarity to the model Hamiltonians used in investigating the microwave ionization of Rydberg states. The problem we are solving is here in the deep quantum regime because of the high frequency and the strongly bound states–just the opposite of the microwave problem [26]. Naturally, the applicability of classical mechanics in this regime is more of a surprise than in the microwave problem.
[26] G. Casati *et al.*, Phys. Rep. **154**, 77 (1987).
[27] B. Hu, J. Liu, and S.-G. Chen, Phys. Lett. A **236**, 533 (1997).
[28] K. A. Mitchell, Physica D **238**, 737 (2009).